Polymer Chemistry

Self-Assembly Behavior of Oligo(ethylene glycol) Substituted Polycaprolactone Homopolymers

Journal:	*Polymer Chemistry*
Manuscript ID	PY-ART-04-2021-000483.R1
Article Type:	Paper
Date Submitted by the Author:	18-May-2021
Complete List of Authors:	Stefan, Mihaela; Univ Texas Dallas, Chemistry and Biochemistry; University of Texas at Dallas Calubaquib, Erika; University of Texas at Dallas, Chemistry Soltantabar, Pooneh ; Univ Texas Dallas, Chemistry and Biochemistry Wang, Hanghang; University of Texas at Dallas, Chemistry Shin, Heejin; University of Texas at Dallas, Chemistry and Biochemistry Flores, Alfonso; Univ Texas Dallas, Chemistry and Biochemistry Biewer, Michael; University of Texas at Dallas, Department of Chemistry

ARTICLE

Self-Assembly Behavior of Oligo(ethylene glycol) Substituted Polycaprolactone Homopolymers

Received 00th January 20xx,
Accepted 00th January 20xx

DOI: 10.1039/x0xx00000x

Erika L. Calubaquib,[a] Pooneh Soltantabar,[b] Hanghang Wang,[a] Heejin Shin,[a] Alfonso Flores,[a] Michael C. Biewer,[a] and Mihaela C. Stefan[a,b,*]

Amphiphilic homopolymers are gaining importance due to their easy synthesis compared to copolymers and their ability to assemble into various nanostructures. The majority of reported amphiphilic homopolymers have a non-biodegradable backbone, are charged, and are dependent on pH for assembly. In this work, we report the self-assembly behavior of non-ionic amphiphilic poly(γ-oligo(ethylene glycol)-ε-caprolactone) homopolymers (PME_xCL, x = 2, 3, and 4), and a novel poly(*N*-dodecyl-*N*-(2-(2-(2-methoxyethoxy)ethoxy)ethyl)-7-oxoxepane-4-carboxamide (PME_3DDCL) homopolymer. These synthesized amphiphilic homopolymers readily self-assembled forming micelles in a polar environment. PME_xCL also exhibited thermoresponsivity; hence, several parameters that affect the thermoresponsivity of these polymers were studied, such as degree of polymerization, concentration, heating rate, and length of oligo(ethylene glycol) side chains. The size, morphology, and thermodynamic stability were investigated, and the micelles were loaded with eugenol to explore the possibility of using the micelles for drug encapsulation. These self-assembled homopolymers hold promise for vast applications, particularly in the biomedical field.

Introduction

Amphiphilic block copolymers' self-assembly ability is a well-established and explored field, especially as drug delivery systems. Their inherent ability to self-assemble into different nanostructures is determined by many factors, including the polymer's chemical structure, the balance between the hydrophobic and hydrophilic parts, concentration, and environmental factors.[1-4] With the growing interest in exploring the self-assembly of polymers, homopolymers provide a more straightforward synthetic route and offer a wide array of nanostructures, such as micelles, large compound micelles, hydrated large compound micelles, inverse micelles, flower-like micelles, vesicles, and large compound vesicles.[5-11] These homopolymers have found many applications, including encapsulation, separation, enzyme inhibition, catalysis, and biosensing.[12-16]

There are two strategies to prepare homopolymer self-assemblies: (1) the "monomer-induced" method in which specially designed amphiphilic monomers are polymerized, and (2) the "hydrophobic group-induced" where the hydrophilic homopolymer is sandwiched between two large hydrophobic end-groups that can interact non-covalently to allow assembly.[5] Extensive work on facially amphiphilic monomers has been reported by Thayumanavan et al.[17 18] These monomers are designed to have hydrophilic and hydrophobic functionalities on opposite sides to enable phase segregation upon assembly. The long hydrophobic moiety and hydrophilic carboxylic acid group in the polymer repeating unit could drive the self-assembly of the homopolymers into micelles and inverted micelles in polar and apolar solvents. Moreover, vesicles were formed with subtle changes in the hydrophobic units through the incorporation of carboxylic acid functional group in the long hydrophobic chain.[16] Du and O'Reilly emphasized the importance of hydrophobic end groups in a very hydrophilic homopolymer in inducing self-assembly.[12, 19] For instance, a hydrophilic and charged poly(*N*,*N*-diethylacrylamide) homopolymers having two hydrophobic end groups form well-defined aggregates at low pH, however, there were no assemblies in the homopolymers containing only one hydrophobic end group.[19] Other factors drive the self-assembly of homopolymers, such as solvent, charge, and temperature. A series of amphiphilic poly(2-hydroxy-3-phenoxypropyl acrylate) can form different nanostructures depending on the strength of the inter/intra-polymer H-bonding formed when chain length and cosolvents are modified.[8] Positively charged poly(L-lysine) polyelectrolytes can spontaneously form vesicles in water only when it interacts with negatively charged quantum dots.[20] Poly(2-(2-ethoxy)ethyl acrylate forms vesicles that were mainly stabilized by the charged end group, and the aggregation can be controlled through temperature changes.[21]

A majority of the reported homopolymers were rendered water-soluble through the use of charged functionalities such as carboxylate[16, 19] and ammonium salts,[22, 23] but only a few are reported to be non-ionic.[24-26] The charged functionalities allow the polymers to assemble in response to pH changes, significant for some applications. However, there are also possible

[a] Department of Chemistry and Biochemistry, University of Texas at Dallas, Richardson, TX, USA, 75080
[b] Department of Bioengineering, University of Texas at Dallas, Richardson, TX, USA, 75080
* Corresponding author: mihaela@utdallas.edu
Electronic Supplementary Information (ESI) available: See DOI: 10.1039/x0xx00000x

drawbacks, such as the cytotoxicity exhibited by polycations.[27] Hence, it is desirable to broaden the library of amphiphilic homopolymers that are non-ionic. For non-ionic polymers, oligo(ethylene glycol) (OEG) is employed to impart water solubility and make the polymer thermoresponsive,[25, 28, 29] which is an excellent advantage for the production of smart drug delivery systems, hydrogels, surfaces, etc.

Polymers with an OEG pendant functional groups usually exhibit a lower critical solution temperature (LCST), which means that polymers are soluble below a critical temperature but will undergo a phase transition when the temperature is elevated.[30] Below the LCST, the OEG chains and water form hydrogen bonds resulting in polymer dissolution, but when the temperature is elevated, the hydrophobic interaction of the backbone results in polymer aggregation. Some of the other thermoresponsive polymers that are also commonly used are poly(oligo(ethylene glycol) (meth)acrylate)s,[31, 32] poly(N-isopropylacrylamide),[33, 34] and poly(oxazoline).[35, 36] The OEG side chain, which is in a brush type architecture, being a non-linear analog of poly(ethylene glycol) (PEG) can be an advantage over non-PEG derived polymers due to the long history of PEG for use commercially, in research, and clinical settings.[37]

Our group has reported OEG substituted polycaprolactones (PME_xCL), which are copolymerized with hydrophobic PCL to obtain micelles that are fully biodegradable and exhibit LCST.[38-43] These block copolymers were found to be thermodynamically stable with critical micelle concentration (CMC) ranging from 10^{-2} to 10^{-5} g/L. We were able to encapsulate doxorubicin and polyphenols into the micelle core, which were released in a controlled manner by taking advantage of the thermoresponsivity of the polymers.[44, 45] In this paper, we take advantage of the OEG side chain and PCL backbone to build ten amphiphilic biodegradable homopolymers. Moreover, a novel poly(*N*-dodecyl-*N*-(2-(2-(2-methoxyethoxy)ethoxy)ethyl)-7-oxoxepane-4-carboxamide (PME_3DDCL) polymer, which incorporates both hydrophilic and hydrophobic units in the side chain, is also reported. To investigate the homopolymer's ability to load hydrophobic molecules, eugenol, a well-known antiseptic and anti-inflammatory oil, was utilized. Eugenol is encapsulated in nanoparticles to enhance bioavailability and protection from degradation due to temperature, oxidation, and light.[46, 47]

Results and discussion

The γ-OEG functionalized ε-caprolactone monomers, namely γ-2-(2-methoxyethoxy)ethoxy-ε-caprolactone) (γ-ME_2CL), γ-2-(2-(2-methoxyethoxy)ethoxy)ethoxy-ε-caprolactone) (γ-ME_3CL), and γ-2-(2-(2-(2-methoxyethoxy)ethoxy) ethoxy)ethoxy-ε-caprolactone) (γ-ME_4CL), were prepared similarly to our previously reported method.[45] To synthesize the PME_xCL homopolymers, coordination-insertion ring-opening polymerization was employed using $Sn(Oct)_2$ as the catalyst and BnOH as the initiator (Scheme 1). Polymers with various lengths of OEG side chains were synthesized to tune the cloud point temperature (T_{cp}) of the homopolymers. Through the adjustment of the monomer to the initiator ratio, polymers of various polymerization degrees (DP_n) were generated. To enhance the homopolymer's hydrophobicity, we decided to introduce dodecyl moiety in the side chain through an amide functionality. We hypothesized that this could be a strategy to improve the thermodynamic stability and enhance the loading efficiency of the micelles. The novel amide substituted caprolactone, *N*-dodecyl-*N*-(2-(2-(2-methoxyethoxy)ethoxy)ethyl)-7-oxoxepane-4-carboxamide (γ-ME_3DDCL) was polymerized using triazabicylo[4.4.0]dec-5-ene (TBD). TBD catalyst was used since it has been reported that an efficient polymerization cannot be obtained using $Sn(Oct)_2$.[48] Monomer and polymers were synthesized and characterized by ^{1}H NMR, ^{13}C NMR, ESI-MS (Figure S1-S15), and size exclusion chromatography (SEC).

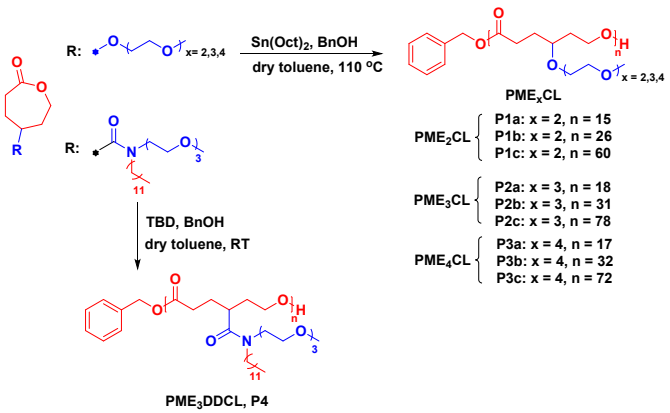

Scheme 1. Synthetic route for the polymerization of γ-substituted caprolactone (PME_2CL: poly(γ-2-(2-methoxyethoxy)ethoxy-ε-caprolactone); PME_3CL: poly(γ-2-(2-(2-methoxyethoxy)ethoxy)ethoxy-ε-caprolactone); PME_4CL: poly(γ-2-(2-(2-(2-methoxyethoxy)ethoxy)ethoxy)ethoxy-ε-caprolactone); PME_3DDCL: poly(*N*-dodecyl-*N*-(2-(2-(2-methoxyethoxy)ethoxy)ethyl)-7-oxoxepane-4-carboxamide))

Table 1 summarizes the molecular weight and polydispersities of the homopolymers. DP_n was estimated from ^{1}H NMR by obtaining the ratio of the integrations of the methylene benzyl protons of the initiator and the methylene protons adjacent to the oxygen in the polymer backbone, which are at ~5.1 ppm and ~4.2 ppm, respectively. The molecular weight was estimated by getting the product of the DP_n and the molecular weight of the monomer then adding the molecular weight of the end group. The molecular weights determined from the SEC were lower compared to the values obtained by ^{1}H NMR analysis. This discrepancy can be attributed to the difference in the hydrodynamic volume of the polymers and the poly(methyl methacrylate) standard used for calibration. All the

resulting polymers show relatively narrow PDI ranging from 1.08 to 1.56. As a representative, the glass transition temperature (T_g) of the polymers **P2c** and **P4** were determined by DSC analysis (Figure S16). T_g values of -65 °C and -49 °C were obtained for **P2c** and **P4**, respectively.

Table 1. Summary of molecular weight and cloud point temperature (T_{cp}) data

Polymer	Monomer	M/I [a]	DP_n [b]	M_n (kg/mol) [c]	M_n (kg/mol) [d]	PDI [d]	T_{cp}, °C [e]	$f_{OEG,\%}$ [f]
P1a	γ-ME_2CL	25	15	3.6	2.9	1.08	58.6	49.7
P1b	γ-ME_2CL	50	26	6.1	3.1	1.08	63.7	50.8
P1c	γ-ME_2CL	100	60	14.0	3.4	1.08	65.3	51.1
P2a	γ-ME_3CL	25	18	5.1	5.2	1.24	61.7	57.6
P2b	γ-ME_3CL	50	31	8.7	5.9	1.23	65.5	58.2
P2c	γ-ME_3CL	100	78	21.0	6.1	1.56	66.0	60.6
P3a	γ-ME_4CL	25	17	5.6	4.2	1.13	84.7	63.0
P3b	γ-ME_4CL	50	32	10.4	5.5	1.15	84.8	63.8
P3c	γ-ME_4CL	100	72	23.2	5.9	1.10	85.8	64.4
P4	γ-ME_3DDCL	50	43	20.4	4.0	1.10	--	40.0*

a) Feed mol ratio of monomer to initiator; b) Degree of polymerization (DP_n) was determined from ^{1}H NMR by from the ratio of the integration of the methylene proton of the initiator and the methylene proton adjacent to the oxygen of the repeating unit; c) Determined from ^{1}H NMR by multiplying the DP_n of the polymer with the MW of the monomer then adding the MW of the end group; d) Determined from SEC using PMMA standard and DMF as eluent; e) Determined from UV-Vis (2.5 mg/mL of polymer in water, n=3); f) Weight fraction of OEG side chains (*amide functionality included)

To confirm the end-group of the polymers, MALDI-TOF mass spectrometry was employed. Figure 1 shows three sets of peaks at an interval of ~232 m/Z. The major series of ions observed (series A) is attributed to the monoisotopic masses of Na^+ adduct of **PME_2CL** having a benzyloxy (BnO) group and an OH group at the initiating and terminating ends, respectively. The minor series of peaks (series B and C) corresponds to the monoisotopic masses of Na^+ adducts of **PME_2CL** with a COOH group and an OH group at each end, which was due to the presence of small amounts of water in the system. **PME_3CL**, **PME_4CL**, and **PME_3DDCL** (Figure S17-S19) show a major series of peaks initiated by the corresponding alcohol, while minor series of peaks are initiated by water. Compared to the other polymers, a water-initiated polymer had a higher percentage in **PME_4CL**, which is expected due to the higher hydrophilicity of its monomer.

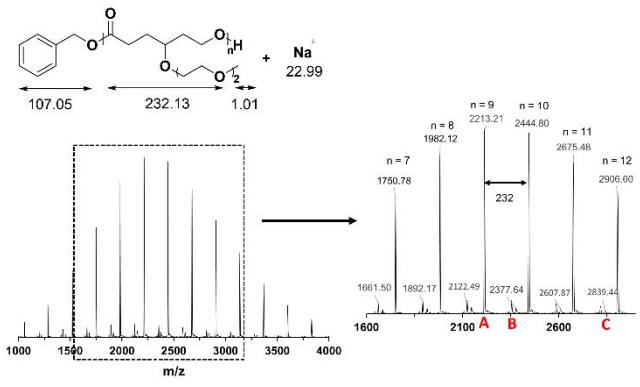

Figure 1. MALDI-ToF mass spectrum of the synthesized PME_2CL (P1a), mole ratio γ-ME_2CL:BnOH:$Sn(Oct)_2$ = 25:1:1

UV-vis spectroscopy was used to measure the T_{cp} of the polymer, which was obtained at the temperature at which the transmittance at 600 nm dropped to 50%. The homopolymers were directly dissolved in water at a range of concentrations from 1 to 10 mg/mL and allowed to equilibrate for 24 h. Shown in Figure 2 are the turbidity curves for polymer **P2a**. In the heating and cooling cycles (Figure 2A), it was observed that the phase transition is reversible (Figure 2A), and a slightly lower cloud point temperature is observed from the cooling curve. This hysteresis can be attributed to the energy barriers when the collapsed OEG chains undergo rehydration.[28] Figure 2B shows that the T_{cp} of the homopolymers is dependent on the concentration, where it increases upon dilution because of the limited intermolecular association.[28] Also, this can be attributed to the limitation in the turbidimetry technique where at low concentrations, the initial stage of phase separation contains small aggregates that can hardly be detected.[49] The same trends were observed for the rest of the polymers. The T_{cp} values in Figure 2C were obtained from the heating ramp of the 2.5 mg/mL concentration of the homopolymer. As DP_n decreases, the homopolymers tend to be more hydrophobic considering the presence of a hydrophobic initiating group, resulting in the shift of the T_{cp} to lower temperature. However, small changes can be observed, which can be attributed to the slight change in the hydrophobic to the hydrophilic ratio of the polymers, as seen in Table 1, where the weight fraction of the OEG side chains is presented. In a previous report, no significant change in T_{cp} was observed with increase in DP_n.[50] In general, a longer OEG chain increases the solubility of the polymer in water, hence an increase in T_{cp}. The turbidity curves of the other representative polymers (**P1b**, **P2b**, and **P3b**) are shown in Figure S20. The T_{cp} of the 1 mg/mL solution of **P3b** cannot be determined since measurement should be performed at higher temperatures. It was previously reported by our group that

ARTICLE

copolymerization of **P1-P3** with benzyloxy-substituted PCL gave T_{cp} values of 15, 41, ad 59 °C, respectively.[45] Copolymerization of **P2** with hydrophobic group-substituted PCL allowed the

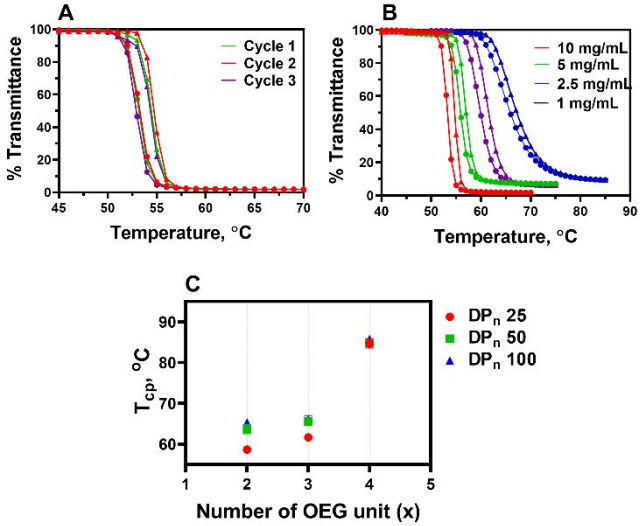

Figure 2. (A and B) Turbidity curves obtained from an aqueous solution of P2a (Δ is heating and ○ is cooling): (A) Polymer was subjected to heating and cooling multiple times; (B) Dependence of T_{cp} on the polymer concentration; and (C) Relationship between number of OEG unit (x), molecular weight, and cloud point.

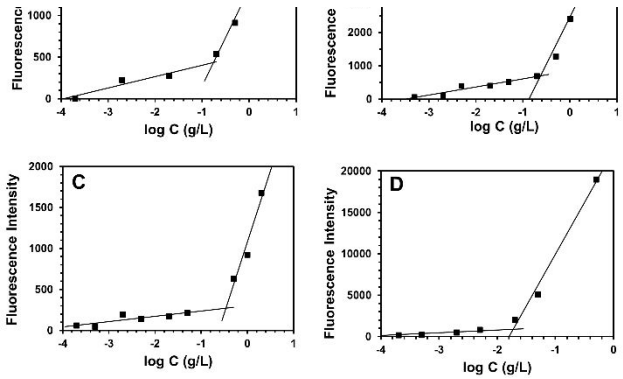

Figure 3. CMC plots obtained from fluorescence spectroscopy using Nile Red as probe: (A) **P1c**, (B) **P2c**, and (C) **P3c**, and (D) **P4**

tuning of T_{cp} values from 29.9 to 54.2 °C.[38-42] Although the T_{cp} of the homopolymers were not in the appropriate range for biological applications, manipulation of the T_{cp} can be performed through the use of more hydrophobic end groups as the polymer initiator or by using a more hydrophobic group in the side chain end group such as ethoxy. For polymer **P4**, there was no transition observed even when the temperature was lowered to 4 °C. For further studies, various alkyl and OEG chains can be integrated into the amide side chain of the homopolymer to tune the property.

To study the effect of the different heating rates on the T_{cp}, 5 mg/mL of **P2b** was heated at 0.5, 1.0, 2.5, and 5.0 °C/min (Figure S21). There was no difference observed when the solution was heated at 0.5 and 1.0 °C/min; however, the T_{cp} shifted to a higher temperature with faster heating. This is due to the relatively slow response of precipitation of polymer chains compared to the heating rate and the lag time in between heating of the sample holder and the solution.[49]

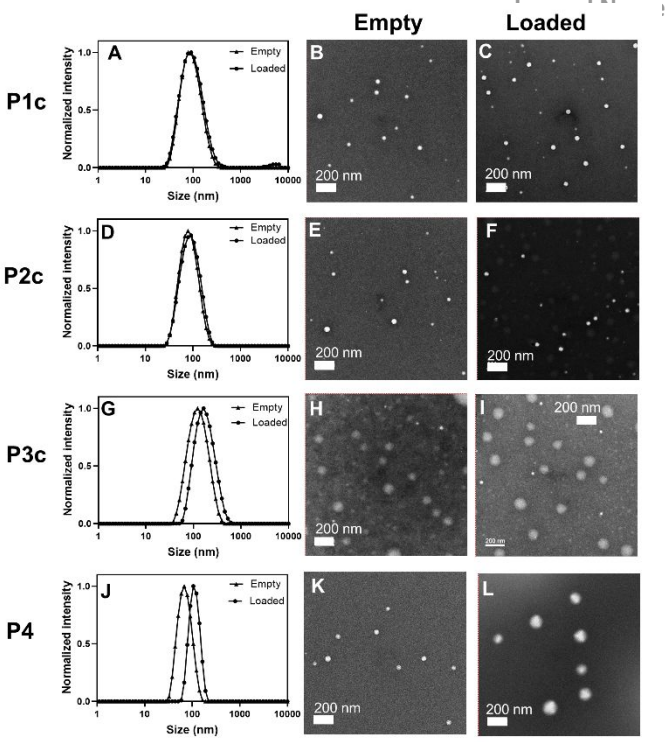

Figure 4. Size and morphology of empty and loaded micelles. Spherical morphologies were observed in the TEM images of the micelles. After loading, a minor increase in size was obtained for **P1c, P2c**, and **P3c,** while a more distinct change was observed for **P4**

The homopolymer's self-assembly ability was investigated through critical micelle concentration (CMC) determination using a hydrophobic Nile Red as a fluorescent probe (Figure 3). In intact micelles, Nile Red exhibits strong fluorescence, but when micelles are destabilized, it becomes minimally fluorescent.[51] The fluorescence intensity at the maximum emission wavelength versus the log of concentration shows an inflection point, which was considered the CMC. The CMC values of the different OEG substituted homopolymers are 2.2 x 10^{-1}, 2.4 x 10^{-1}, and 3.7 x 10^{-1} g/L for **P1c**, **P2c**, and **P3c**, respectively, where increasing the OEG side chain length increases the CMC. A more stable micelle was obtained for **P4** having a CMC of 1.8 x 10^{-2} g/L, which can be due to the more distinct phase segregation of the hydrophilic and hydrophobic moieties in the polymer chain. From our previous work, copolymerization of **P1-P3** with benzyloxy-substituted PCL gave CMC values in the order of 10^{-5} g/L.[45] Moreover, copolymerization of **P2** with unsubstituted PCL or different hydrophobic group-substituted PCL gave CMC values ranging from 1.39 x 10^{-2} to 5.62 x 10^{-4} g/L.[40, 42-44] The high CMC values of the homopolymers, which are typical for homopolymers, can be attributed to the unfavorable entropy of the bending of the hydrophilic groups.[19]

DLS was used to determine the hydrodynamic diameter, size distribution, and zeta potential of the micelles (Table 2). Sizes of 73.2, 68.2, 152.0, and 77.0 nm were estimated for **P1c**, **P2c**, **P3c**, and **P4**, respectively (Figure 4). The large size of **P3c** compared to the other homopolymers could be attributed to the more extended OEG unit in the micelle's corona. To investigate the ability of the micelles to load hydrophobic molecules, eugenol was used as a representative molecule.

Eugenol, a well-known antiseptic, and anti-inflammatory molecule is encapsulated in nanoparticles to enhance its bioavailability. DLS of loaded micelles showed a slight increase for **P1c** (82.0 nm) and **P2c** (75.9 nm) micelles, while a more considerable size change was observed for **P3c** (183.6 nm) and **P4** (133.8 nm) micelles (Figure 4 and Table 2). Spherical micelles were observed based on the TEM images. Smaller sizes were obtained from TEM due to the dehydration of the micelles (Figure 4).[45] The empty and loaded **P1c** and **P2c** micelles and the empty **P4** micelles showed sizes in the range of 50 – 60 nm, while larger sizes were observed for the empty **P3c** micelles and loaded **P3c** and **P4** micelles. A negative zeta potential value was obtained for all the micelles. The zeta potential of **P2c** micelles was comparable to those reported for its copolymers.[39, 40]

As seen in Table 2, an approximate 2.7-fold higher loading was observed for **P4** compared with **P2c**, which has the same length of OEG unit. This could be due to the improved hydrophobic interaction of eugenol and the alkyl moiety of **P4**. The higher loading can also explain why a more considerable change in size was obtained after the loading of **P4**. Encapsulation efficiencies of 11.7%, 18.3%, 21.9%, and 48.3% were obtained for **P1c, P2c, P3c,** and **P4**, respectively.

Table 2. Characteristics of empty and loaded micelles

	Empty		Loaded		Eugenol loading capacity (%)
	Particle size, nm (Dispersity)	Zeta potential, mV	Particle size, nm (Dispersity)	Zeta potential, mV	
P1c	73.2 (0.44)	-7.9	82.0 (0.30)	-8.3	1.1
P2c	68.2 (0.26)	-11.8	75.9 (0.20)	-12.8	1.8
P3c	152.0 (0.39)	-10.3	183.6 (0.39)	-11.0	2.2
P4	77.0 (0.12)	-10.4	133.8 (0.10)	-9.9	4.8

DLS was used to determine the hydrodynamic diameter, size dispersity, and zeta potential of micelles in water

One aspect that should be considered is the stability of the micelles upon storage. Being the most thermodynamically stable, empty and loaded micelles of **P4** were studied. From the DLS analysis, no changes in size and dispersity were observed for 21 days for the micelles stored at room temperature, showing the micelles' stability (Figure 5).

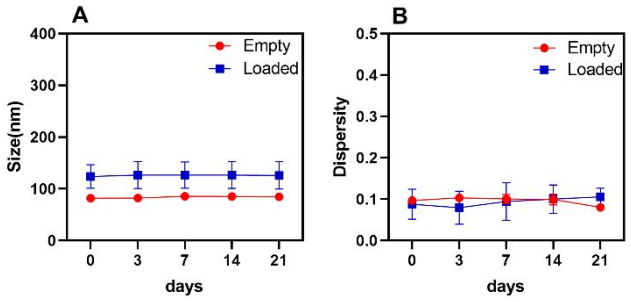

Figure 5. Stability of 1 mg/mL of **P4** empty and loaded micelles in water: (A) size and (B) dispersity. DLS was used to monitor the size and dispersity of the empty and loaded micelles stored at room temperature

Conclusion

To conclude, we report the thermoresponsivity and the homopolymer self-assembly of non-ionic amphiphilic PME_xCL polymers. Side-chain length impacts the cloud point temperature in an aqueous solvent, but the nanostructure's morphology remains unchanged. Adding a hydrophobic moiety, such as the dodecyl group in **PME_3DDCL (P4)**, in the side chain enhances the thermodynamic stability by ~13 fold and the ability of the homopolymer to load hydrophobic molecules by ~2.7 fold in comparison to **P2c**, which has the same length of OEG side chain. These homopolymers could be used to prepare micelles for possible applications in the biomedical field, particularly as drug carriers.

Experimental Section

Synthesis

Monomer synthesis and characterization are shown in the SI (Scheme S1).

Procedure for the synthesis of poly(γ-2-(2-methoxyethoxy)ethoxy-ε-caprolactone), PME_2CL (**P1b**): γ-ME_2CL (1.0 g, 4.3 mmol) was dried with CaH_2 then weighed into a Schlenk flask inside the glove box. Solutions of $Sn(Oct)_2$ (35.0 mg, 8.6 x 10^{-2} mmol) and benzyl alcohol (BnOH) (9.3 mg, 8.6 x 10^{-2} mmol) in toluene were added to the flask then heated at 110 °C. The polymers were obtained by precipitation in hexane. The reaction was repeated using 25 : 1 : 1 (**P1a**) and 100 : 1 : 1 (**P1c**) ratio of monomer : catalyst : initiator. PME_2CL: ^{1}H NMR (500 MHz, $CDCl_3$) δ: 1.75-1.90 (m, 4H), 2.37-2.39 (t, 2H), 3.37 (s, 3H), 3.45-3.60 (m, 9H), 4.15-4.17 (t, 2H). ^{13}C NMR (500 MHz, $CDCl_3$) δ: 29.06, 29.76, 33.09, 59.03, 61.32, 68.54, 70.54, 70.74, 71.95, 75.83, 173.48.

*Procedure for the synthesis of poly(γ-2-(2-(2-methoxyethoxy)ethoxy)ethoxy-ε-caprolactone), PME_3CL (**P2a-c**) and poly(γ-2-(2-(2-(2-methoxyethoxy)ethoxy)ethoxy)ethoxy-ε-caprolactone), PME_4CL (**P3a-c**)*: Similar procedure was followed to synthesize PME_3CL and PME_4CL with a feed mol ratio of 25 : 1 : 1, 50 : 1 : 1, and 100 : 1 : 1. (a) PME_3CL: ^{1}H NMR (500 MHz, $CDCl_3$) δ: 1.70-1.90 (m, 4H), 2.37-2.40 (t, 2H), 3.37 (s, 3H), 3.45-3.65 (m, 13H), 4.15-4.20 (t, 2H). ^{13}C NMR (500 MHz, $CDCl_3$) δ: 29.21, 29.89, 33.23, 59.15, 61.46, 68.67, 70.67, 70.75, 70.85, 72.07, 75.93, 173.59. (b) PME_4CL: ^{1}H NMR (500 MHz, $CDCl_3$) δ: 1.76-1.85 (m, 4H), 2.37-2.39 (t, 2H), 3.37 (s, 3H), 3.45-3.65 (m, 17H), 4.15-4.17 (t, 2H). ^{13}C NMR (500 MHz, $CDCl_3$) δ: 29.19, 29.88, 33.21, 59.14, 61.45, 68.65, 70.63, 70.71, 70.73, 70.83, 72.07, 75.93, 173.56.

Procedure for the synthesis of poly(N-dodecyl-N-(2-(2-(2-methoxyethoxy)ethoxy)ethyl)-7-oxoxepane-4-carboxamide), PME3DDCL, **P4**

Triazabicylo[4.4.0]dec-5-ene (TBD) (4.7 mg, 0.03 mmol, 2 mol% relative to the monomer) and BnOH (3.7 mg, 0.03 mmol) in dry toluene were mixed into a Schlenk flask. The mixture was stirred for 30 min followed by the addition of γ-ME_3DDCL monomer

(0.8 g, 1.7 mmol), which was dried first with CaH_2. The reaction stirred at room temperature then halted by air exposure. The polymers were obtained by dissolving in THF then precipitation in hexane. ^{1}H NMR (500 MHz, $CDCl_3$) δ: 0.85-0.89 (t, 3H), 1.22-1.31 (m, 18H), 1.46-1.54 (m, 2H), 1.67-1.80 (m, 2H), 1.87-2.01 (m, 2H), 2.18-2.33 (m, 2H), 2.73-2.88 (m, 1H), 3.25-3.39 (m, 5H), 3.44-3.66 (m, 12H), 3.93-4.06 (m, 2H). ^{13}C NMR (500 MHz, $CDCl_3$) δ: 14.25, 22.82, 27.07, 27.26, 27.78, 29.49, 29.55, 29.75, 29.79, 29.82, 31.38, 31.55, 31.69, 32.05, 37.00, 46.44, 46.92, 47.40, 49.23, 59.15, 62.61, 62.73, 69.33, 69.63, 70.55, 70.66, 70.71, 70.76, 70.82, 72.04, 72.08, 172.92, 173.08, 173.96, 174.04.

Measurement of cloud point temperature

The polymer was dissolved in water and equilibrated for 24 h at room temperature before measurement. The percent transmittance at 600 nm was obtained at 0.5 ˚C/min heating and cooling rates, unless otherwise stated, using a quartz cuvette with a path length of 1.0 cm. The point of the 50% drop in transmittance in the heating run was taken as the cloud point temperature.

Critical micelle concentration measurement

The CMC of the homopolymers was determined using Nile Red fluorescent probe. The polymer in various concentrations and a constant amount of Nile Red (final concentration = 3.1 x 10^{-5} M), both in THF, were mixed. The mixture was added to water, and THF was evaporated through agitation. The samples were subjected to fluorescence spectroscopy to identify the CMC. The emission spectra were obtained from 570 – 750 nm with an excitation wavelength of 550 nm. The CMC was determined at the inflection point on the plots of fluorescence intensity at the maximum emission wavelength as a function of the polymer concentration, as previously described by Moller et al.[51]

Preparation of micelles

The homopolymer (5.0 mg) was dissolved in THF (1 mL), then added dropwise to water (5 mL) while homogenizing. After 30 min, the solution was then transferred to a shaker to evaporate THF. The solution was loaded into a dialysis bag with a MW cut-off of 3500 Da and dialyzed for 24 h, then filtered with a nylon syringe filter (0.45 µm).

Loading with eugenol

The eugenol-loaded micelles were prepared similarly by dissolving both the homopolymer and eugenol in THF. The solution was dialyzed for 24 h, then filtered using a 0.45 µm nylon syringe filter. To determine the drug loading capacity (DLC) and encapsulation efficiency (EE), the lyophilized sample was dissolved in water, followed by collapsing the micelles through the addition of DMSO. The actual concentration of eugenol was determined using the following equations:

$$\% \text{ DLC} = \frac{\text{Weight of eugenol loaded (mg)}}{\text{Weight of the polymer used (mg)}} \text{x } 100 \qquad (1)$$

$$\% \text{ EE} = \frac{\text{Weight of eugenol loaded (mg)}}{\text{Total weight of eugenol (mg)}} \text{x } 100 \qquad (2)$$

Conflicts of interest

There are no conflicts to declare.

Acknowledgments

The authors would like to thank Arezoo Shahrivarkevishahi and Alejandra Durand-Silva for their help with MS and DSC analysis. Financial support from the Welch Foundation (AT-1740), National Science Foundation (CHE-1609880) is gratefully acknowledged. M.C.S. thanks the endowed chair support from the Eugene McDermott Foundation. This project was partially funded by the University of Texas at Dallas Office of Research through the Core Facility Voucher Program.

References

1. Y. Mai and A. Eisenberg, *Chem. Soc. Rev.*, 2012, **41**, 5969-5985.
2. B. Zhang, H. Zhang, Y. Li, J. N. Hoskins and S. M. Grayson, *ACS Macro Lett.*, 2013, **2**, 845-848.
3. M. Karayianni and S. Pispas, in *Fluorescence Studies of Polymer Containing Systems*, ed. K. Procházka, Springer International Publishing, Cham, 2016, pp. 27-63.
4. E. Konishcheva, D. Daubian, J. Gaitzsch and W. Meier, *Helv. Chim. Acta*, 2018, **101**, e1700287.
5. J. Zhang, K. Liu, K. Müllen and M. Yin, *Chem. Commun.*, 2015, **51**, 11541-11555.
6. T. Kubo, C. P. Easterling, R. A. Olson and B. S. Sumerlin, *Polym. Chem.*, 2018, **9**, 4605-4610.
7. V. V. Vasilevskaya and E. N. Govorun, *Polym. Rev.*, 2019, **59**, 625-650.
8. Y. Zhu, L. Liu and J. Du, *Macromolecules*, 2013, **46**, 194-203.
9. L.-H. Wang, Z.-D. Zhang, C.-Y. Hong, X.-H. He, W. You and Y.-Z. You, *Adv. Mater.*, 2015, **27**, 3202-3207.
10. L.-H. Wang, T. Wu, Z. Zhang and Y.-Z. You, *Macromolecules*, 2016, **49**, 362-366.
11. L.-H. Wang, W. Ting and Y.-Z. You, *Polym. Chem.*, 2015, **6**, 4972-4977.
12. T. Liu, W. Tian, Y. Zhu, Y. Bai, H. Yan and J. Du, *Polym. Chem.*, 2014, **5**, 5077-5088.
13. S. R. Mane, V. Rao N, K. Chaterjee, H. Dinda, S. Nag, A. Kishore, J. Das Sarma and R. Shunmugam, *Macromolecules*, 2012, **45**, 8037-8042.
14. J. P. Patterson, P. Cotanda, E. G. Kelley, A. O. Moughton, A. Lu, I. I. I. T. H. Epps and R. K. O'Reilly, *Polym. Chem.*, 2013, **4**, 2033-2039.
15. F. Wang, A. Gomez-Escudero, R. R. Ramireddy, G. Murage, S. Thayumanavan and R. W. Vachet, *J Am Chem Soc*, 2013, **135**, 14179-14188.
16. T. S. Kale, A. Klaikherd, B. Popere and S. Thayumanavan, *Langmuir*, 2009, **25**, 9660-9670.

17. S. Basu, D. R. Vutukuri and S. Thayumanavan, *J Am Chem Soc*, 2005, **127**, 16794-16795.
18. E. N. Savariar, S. V. Aathimanikandan and S. Thayumanavan, *J Am Chem Soc*, 2006, **128**, 16224-16230.
19. J. Du, H. Willcock, J. P. Patterson, I. Portman and R. K. O'Reilly, *Small*, 2011, **7**, 2070-2080.
20. J. N. Cha, H. Birkedal, L. E. Euliss, M. H. Bartl, M. S. Wong, T. J. Deming and G. D. Stucky, *J Am Chem Soc*, 2003, **125**, 8285-8289.
21. L. Fan, H. Lu, K. Zou, J. Chen and J. Du, *Chem. Commun.*, 2013, **49**, 11521-11523.
22. L. Arnt and G. N. Tew, *J Am Chem Soc*, 2002, **124**, 7664-7665.
23. S. Colak, C. F. Nelson, K. Nüsslein and G. N. Tew, *Biomacromolecules*, 2009, **10**, 353-359.
24. K. S. Sharma, G. Durand, F. Gabel, P. Bazzacco, C. Le Bon, E. Billon-Denis, L. J. Catoire, J.-L. Popot, C. Ebel and B. Pucci, *Langmuir*, 2012, **28**, 4625-4639.
25. Y. Wang, A. M. Alb, J. He and S. M. Grayson, *Polym. Chem.*, 2014, **5**, 622-629.
26. Y. Kimura, M. Ouchi and T. Terashima, *Polym. Chem.*, 2020, **11**, 5156-5162.
27. B. D. Monnery, M. Wright, R. Cavill, R. Hoogenboom, S. Shaunak, J. H. G. Steinke and M. Thanou, *Int. J. Pharm.*, 2017, **521**, 249-258.
28. R. Chen, Z. Xiang, Y. Xia, Z. Ma, Q. Shi, S.-C. Wong and J. Yin, *Macromol Rapid Commun*, 2020, **41**, 2000206.
29. A. Yiu, D. Simchuk and J. Hao, *Macromol Chem Phys*, 2020, **221**, 2000136.
30. J.-F. Lutz, K. Weichenhan, Ö. Akdemir and A. Hoth, *Macromolecules*, 2007, **40**, 2503-2508.
31. B. Peng, N. Grishkewich, Z. Yao, X. Han, H. Liu and K. C. Tam, *ACS Macro Lett.*, 2012, **1**, 632-635.
32. I. Akar, R. Keogh, L. D. Blackman, J. C. Foster, R. T. Mathers and R. K. O'Reilly, *ACS Macro Lett.*, 2020, **9**, 1149-1154.
33. X. Li, H. ShamsiJazeyi, S. L. Pesek, A. Agrawal, B. Hammouda and R. Verduzco, *Soft Matter*, 2014, **10**, 2008-2015.
34. G.-F. Luo, W.-H. Chen and X.-Z. Zhang, *ACS Macro Lett.*, 2020, **9**, 872-881.
35. O. Sedlacek, D. Bera and R. Hoogenboom, *Polym. Chem.*, 2019, **10**, 4683-4689.
36. D. Daubian, J. Gaitzsch and W. Meier, *Polym. Chem.*, 2020, **11**, 1237-1248.
37. D. Y. Joh, Z. Zimmers, M. Avlani, J. T. Heggestad, H. B. Aydin, N. Ganson, S. Kumar, C. M. Fontes, R. K. Achar, M. S. Hershfield, A. M. Hucknall and A. Chilkoti, *Adv. Healthc. Mater.*, 2019, **8**, 1801177.
38. J. Hao, J. Servello, P. Sista, M. C. Biewer and M. C. Stefan, *J. Mater. Chem.*, 2011, **21**, 10623-10628.
39. Y. Cheng, J. Hao, L. A. Lee, M. C. Biewer, Q. Wang and M. C. Stefan, *Biomacromolecules*, 2012, **13**, 2163-2173.
40. J. Hao, Y. Cheng, R. J. K. U. Ranatunga, S. Senevirathne, M. C. Biewer, S. O. Nielsen, Q. Wang and M. C. Stefan, *Macromolecules*, 2013, **46**, 4829-4838.
41. E. A. Rainbolt, K. E. Washington, M. C. Biewer and M. C. Stefan, *J Mater Chem B*, 2013, **1**, 6532-6537.
42. E. A. Rainbolt, J. B. Miller, K. E. Washington, S. A. Senevirathne, M. C. Biewer, D. J. Siegwart and M. C. Stefan, *J Mater Chem B*, 2015, **3**, 1779-1787.
43. K. E. Washington, R. N. Kularatne, J. Du, M. J. Gillings, J. C. Webb, N. C. Doan, M. C. Biewer and M. C. Stefan, *J Poly Sci A Polym Chem*, 2016, **54**, 3601-3608.
44. K. E. Washington, R. N. Kularatne, J. Du, Y. Ren, M. J. Gillings, C. X. Geng, M. C. Biewer and M. C. Stefan, *J Mater Chem B*, 2017, **5**, 5632-5640.
45. P. Soltantabar, E. L. Calubaquib, E. Mostafavi, M. C. Biewer and M. C. Stefan, *Biomacromolecules*, 2020, **21**, 1427-1436.
46. A. Joardar, G. Meher, B. P. Bag and H. Chakraborty, *J. Mol. Liq.*, 2020, **319**, 114336.
47. C. Valencia-Sullca, M. Jiménez, A. Jiménez, L. Atarés, M. Vargas and A. Chiralt, *Polym Int*, 2016, **65**, 979-987.
48. L. Wen, S. Zhang, Y. Xiao, J. He, S. Zhu, J. Zhang, Z. Wu and M. Lang, *Macromolecules*, 2020, **53**, 5096-5104.
49. Q. Zhang, C. Weber, U. S. Schubert and R. Hoogenboom, *Mater. Horiz.*, 2017, **4**, 109-116.
50. K. Wang, Q. Liu, G. Liu and Y. Zeng, *Polymer*, 2020, **203**, 122746.
51. T. Trimaille, K. Mondon, R. Gurny and M. Möller, *Int. J. Pharm.*, 2006, **319**, 147-154.